Robust Estimation of Planar Surface Orientation with Continuous Wavelet Transform

Chun-Shien Lu†, Wen-Liang Hwang‡, and Pau-Choo Chung†

† Department of Electrical Engineering, National Cheng Kung University, Taiwan

‡ Institute of Information Science, Academia Sinica, Taipei, Taiwan

Abstract

We propose a new method to estimate the surface orientation of a planar texture under perspective projection based on the ridge surface of 2D continuous wavelet transform (CWT) with rotations. We show that textural information giving the perception of surface orientation can be characterized from ridge surfaces in the space/frequency space. Three variants of ridge detection algorithm are presented. In order to deal with the weakly-ordered and disordered textures, robust regression method (RANSAC) is introduced to solve the problem. A closed-form solution is derived to determine surface orientation. The effectiveness of our method are demonstrated on several real-world textured images.

Corresponding address:

Wen-Liang Hwang

Institute of Information Science, Academia Sinica,

Nankang, Taipei, Taiwan, R.O.C.

E-mail: whwang@iis.sinica.edu.tw

1 Introduction

It had been pointed out [11] that texture variations provide important cues in visual perception of three dimensional structures from a monocular image. In computer vision and image processing, this problem has received much attention and is called shape from texture, even though it is the orientation of a planar surface instead of the shape of a curved surface that is being computed. The reason may be that a curved surface can be approximately recovered provided that the orientation of the planes tangent to the surface are estimated. The orientation of a planar surface are the slant angle, which determines the degree of obliqueness of the surface, and the tilt angle, which is the direction towards which the texture in the image plane inclines most rapidly.

The main difficulty in solving the shape from texture problem is how to characterize the texture variations of perceived images. In the literature, many authors [1][5][4] used texture features such as the texels or edges as the representation of texture variations. However, it is well-known that the detection of texels and edges are not much reliable. The textural variations is better to be characterized by the space/frequency representation, since it has been shown that textures are distorted locally and non-linearly [16][12]. In the past, some space/frequency representations [3][13][14][18][19] had been adopted. We chose the continuous wavelet transform with rotations, in particular the Morlet wavelet, because it gives a dense sampling in the space/frequency domain and optimizes both spatial resolution and frequency resolution simultaneously. In our previous papers [16][12], analytical solution has been proposed to estimate the planar surface orientation of strongly ordered texturs, i.e., textures with regular variations. In this paper, a robust method is proposed for textures with less regular structure such as weakly ordered or disordered textures described in Rao's book [17]. A ridge detection algorithm together with a robust regression method based on random sample consensus [10], are proposed in estimating the surface orientation of complex planar textures. In the past, to the best of our knowledge, only Kube [15] can estimate the surface slant of random textures. He used orthographical projection model and assumed isotropic textures. Our method differs from his in that we use perspective projection model and homogeneous textures are assumed.

In addition, the used texture models are different: we used sinusoidal texture model whereas they used fractional Brownian plane. Furthermore, our method can estimate tilt angle while his method can not.

The rest of this paper is arranged as following. In Sec. 2, some background for the two-dimensional continuous wavelet transform is briefly reviewed. In Sec. 3, we propose three algorithms to detect ridge surfaces. In Sec. 4, we explain why the surface orientation is derivable from ridge surfaces. A closed-form solution in computing the tilt and the slant angles is provided. In Sec. 5, a hybrid of ridge detection and robust fitting algorithm is proposed. Finally, the experiments and conclusions are summarized in Sections 6 and 7, respectively.

2 Continuous Wavelet Transform

A complex-valued function $\psi(\mathbf{x}) \in L^2(\mathcal{R}^2)$ is called a wavelet if the double integral is zero: $\int_{\mathcal{R}^2} \psi(\mathbf{x}) d\mathbf{x} = 0$. Let $\psi_{(\mathbf{b},\, s,\, \theta)}(\mathbf{x})$ be obtained by the translation, scaling, and rotation of $\psi(\mathbf{x})$:

$$\psi_{(\mathbf{b},\, s,\, \theta)}(\mathbf{x}) = \frac{1}{s^2}\psi(\mathbf{r}_{-\theta}\frac{\mathbf{x}-\mathbf{b}}{s}),$$

where $\mathbf{b} \in \mathcal{R}^2$, $s > 0$, and $\theta \in [0, 2\pi)$ are translation, scaling, and rotation parameters, respectively. Also,

$$\mathbf{r}_\theta = \begin{pmatrix} cos\theta & -sin\theta \\ sin\theta & cos\theta \end{pmatrix}$$

is the rotation matrix of the angle θ. The two-dimensional continuous wavelet transform [2] of $f(\mathbf{x})$ is defined simply as the convolution product with $\psi_{(\mathbf{b},\, s,\, \theta)}(\mathbf{x})$:

$$(\mathcal{W}f)(\mathbf{b}, s, \theta) = \frac{1}{s^2}\int_{I\!R^2} f(\mathbf{x})\overline{\psi(\mathbf{r}_{-\theta}\frac{\mathbf{x}-\mathbf{b}}{s})}d\mathbf{x} = \int_{I\!R^2} \hat{f}(\mathbf{w})\overline{\hat{\psi}(s\mathbf{r}_{-\theta}\mathbf{w})}e^{-j(\mathbf{w}^T\mathbf{b})}d\mathbf{w},$$

where $\overline{\psi(\mathbf{x})}$ denotes the complex conjugate of $\psi(\mathbf{x})$. If the Fourier transform of the wavelet $\psi(\mathbf{x})$ is localized at the frequency $\mathbf{k_0}$, the wavelet transform coefficient at $(\mathbf{b}, s, \theta)$ measures the frequency content of $f(\mathbf{b})$ at $\mathbf{w} = \mathbf{r}_\theta \mathbf{k_0}/s$. In other words, there is a natural association of the polar coordinate (s^{-1}, θ) and the frequency of $\psi_{(\mathbf{b},\, s,\, \theta)}(\mathbf{x})$ at $\mathbf{b}$. We also showed in [12] that the squared-modulus $(\mathcal{W}f)^2(\mathbf{b}, s, \theta)$ can be interpreted as energy density.

3 Ridge Detection

We adopt the texture model [6] represented in terms of a superposition of amplitudes $\{A_k(\mathbf{x})\}$, frequencies $\{\mathbf{\Omega}_k(\mathbf{x})\}$, and phases $\{p_k\}$:

$$f(\mathbf{x}) = \sum_{k \in I(\mathbf{x})} A_k(\mathbf{x}) \cos(\mathbf{\Omega}_k^T(\mathbf{x}) + p_k), \tag{1}$$

where $k \in I(\mathbf{x})$ implying that the kth amplitde in $\{A_k(\mathbf{x})\}$, the kth frequency in $\{\mathbf{\Omega}_k(\mathbf{x})\}$, and the kth phase in $\{p_k\}$ appear at $f(\mathbf{x})$.

The continuous wavelet transform is used to reliably extract the different frequency components of the modulation model. Let us take the wavelet transform of $f(\mathbf{x})$ [12]:

$$\begin{aligned}(\mathcal{W}f)(\mathbf{b}, s, \theta) &= \sum_{k \in I(\mathbf{b})} A_k \frac{1}{s^2} \int_{I\!R^2} \cos(\mathbf{\Omega}_k^T \mathbf{x} + p_k) \overline{\psi_M(\mathbf{r}_{-\theta} \frac{\mathbf{x} - \mathbf{b}}{s})} d\mathbf{x} \\ &= \sum_{k \in I(\mathbf{b})} \frac{A_k}{2} \hat{\psi}_M(s \mathbf{r}_{-\theta} \mathbf{\Omega}_k) e^{-j(\mathbf{\Omega}_k^T \mathbf{b} + p_k)}.\end{aligned}$$

Since $\hat{\psi}_M(\mathbf{w})$ is concentrated at the frequency $\mathbf{k_0}$, the k-th frequency component $\mathbf{\Omega}_k$ of $f(\mathbf{x})$ will be concentrated around $\mathbf{r}_{\theta_k} \mathbf{k_0} / s_k$, where θ_k is the angle between $\mathbf{k_0}$ and $\mathbf{\Omega_k}$, and s_k^{-1} is the magnitude multiplier in order to scale $||\mathbf{k_0}||$ to $||\mathbf{\Omega_k}||$.

In such case, the texture energy at $(\mathbf{b}, s, \theta)$ is approximately the summation of the energy of each individual component:

$$|(\mathcal{W}f)(\mathbf{b}, s, \theta)|^2 \approx \sum_{k \in I(\mathbf{b})} \frac{A_k^2}{4} \left| \hat{\psi}_M(s \mathbf{r}_{-\theta} \mathbf{\Omega}_k) \right|^2. \tag{2}$$

Eq. 2 indicates that the texture energy at $\mathbf{b}$ is concentrated around $|I(\mathbf{b})|$ different frequency components. In polar coordinate (s^{-1}, θ) , they are concentrated around $(\frac{||\mathbf{\Omega}_k||}{||\mathbf{k_0}||}, \theta_k)$ correspondingly. In this paper, we use the following algorithm to effectively extract these points of energy concentration. We select points which are the squared-modulus local maxima among θ and s for any fixed $\mathbf{b}$. Let $\mathcal{N}(x)$ contain the neighborhood of the argument x, including x; then $(\mathbf{b}, s_0, \theta_0)$ is selected if

$$\forall\, \mathcal{N}(s_0)\ \ \forall\, \mathcal{N}\ (\theta_0)\ \ \ |(\mathcal{W}f)(\mathbf{b}, s_0, \theta_0)|^2 \geq |(\mathcal{W}f)(\mathbf{b}, \mathcal{N}(s_0), \mathcal{N}(\theta_0))|^2.$$

It is not hard to realize that the set of energy aggregation points $(\mathbf{b}, s = \frac{||\mathbf{k_0}||}{||\mathbf{\Omega}_k||}, \theta_k)$ is kept by using this simple process. One can then read off from these points important local parameters about the spatial frequency $\mathbf{\Omega}_k$. It is worth noting that the energy aggregation points obtained by our algorithm characterize exactly the local frequency of our texture model [9].

Algorithm 1: *Single ridge detection*

If the neighborhood of a pixel is defined for all voices and angles, there is only one representative frequency for each pixel. We call the detected ridge as the "single ridge". The single ridge is particular suitable for textures with widely separately spectrums. In our previous work [16], we had successfully used single ridge for estimating surface orientation.

Algorithm 2: *Multiple ridges detection*

If the textured image contains several frequencies which are not widely separately, the detected single ridge will not be meaningful since different frequencies contribute to the ridge. For this case, meaningful ridge surfaces should be constructed from ridge points by "continuity" criterion. The neighborhood of a pixel is a narrow interval. The detailed algorithm connecting the ridge points is described as follows:

Multi-ridge detection

1. Unmark all the ridge points.

2. Let $(\mathbf{b}, s, \theta)$ be an unmarked ridge point p and S_i be a new ridge surface.

3. Assign the unmarked neighboring ridge points of p to S_i and mark them. The neighboring ridge points of p are all the ridge points that are neighbors to $(\mathbf{b}, s, \theta)$ in spatial frequency space. In implementation, we adopt the common eight neighborhood for pixel $\mathbf{b}$. The neighborhood of scale s is one voice away from s. Similarly, the neighboring angle of θ is simply $\delta\theta$ degrees away from θ.

4. Repeat the second step until there is no unmarked ridge point.

Based on this process, the frequency information of a textured image forms disjoint ridge surfaces in the continuous wavelet transform. Fig. 1(a) shows a picture of a scene. One observes the slanting building from the decreasing window size. Fig. 1(b) is the scale map

where the maximal modulus occurs at each pixel **b** (called single ridge). Figs. 1(c)-(f) show the scales of multiple ridge surfaces. Fig. 1(c) shows the ridge surface corresponding to the slanting building, where the ridge surface tilts horizontally. Fig. 1(d) shows the ridge surface of vertical structures of the building. Figs. 1(e) and (f) correspond to the road and the cars in front of the building.

4 Projection Model and Estimation of Surface Orientation

4.1 The Viewing Geometry

We choose coordinate systems that have been adopted in [18]. Let the coordinate systems of the world (x_w,y_w,z_w), of the surface plane (x_s,y_s,z_s), and of the image plane (x_i,y_i,z_i) be depicted in Fig. 2. The slant angle ρ is defined as the angle between z_s and z_i, which takes non-negative values between 0° and 90°. Furthermore, the angle between the x_i axis and the projection of the surface normal, i.e. z_s, into the image plane is defined as the tilt angle τ which takes values between -180° and 180°. The slant-tilt combination represents the surface orientation of a planar texture.

The relationship between above coordinate systems of a surface plane and the image plane under the perspective projection model have been derived in [**?**], given by

$$\begin{bmatrix} x_s \\ y_s \end{bmatrix} = \frac{z_w}{f} \begin{bmatrix} \sec\rho & 0 \\ 0 & 1 \end{bmatrix} \begin{bmatrix} \cos\tau & \sin\tau \\ -\sin\tau & \cos\tau \end{bmatrix} \begin{bmatrix} x_i \\ y_i \end{bmatrix}, \tag{3}$$

where

$$\frac{z_w}{f} = \frac{z_0}{\tan\rho(x_i\cos\tau + y_i\sin\tau) + f}. \tag{4}$$

4.2 Projection of Spatial Frequency

The spatial frequency of surface textures when viewed from the projected image will be subjected to certain distortions according to the projective effects. For the moment, we assume

that the tilt angle τ have been derived, hence the rotation matrix $\mathbf{r}_\tau$ is known. Let $\mathbf{x_i} = [x_i \;\; y_i]^T$, and $\mathbf{x_s} = [x_s \;\; y_s]^T$ be coordinates of the image plane and of surface plane, respectively. We denote $\mathbf{x} = [x_i \cos\tau - y_i \sin\tau \;\; x_i \sin\tau + y_i \cos\tau]^T$, the coordinate of new image plane obtained by applying the rotation matrix $\mathbf{r}_\tau$ to $\mathbf{x_i}$. After substituting Eq. (3) into the texture model given in Eq. (**??**), we obtain the projected texture in image plane:

$$g(\mathbf{x}) = \sum_{k \in I(\mathbf{x})} A_k \cos(\mathbf{\Omega}_k^T \frac{z_w}{f} \begin{bmatrix} \sec\rho & 0 \\ 0 & 1 \end{bmatrix} \mathbf{x} + p_k). \tag{5}$$

Let the frequency vector $\mathbf{\Omega}_k = [u_k \;\; v_k]$; we have

$$\begin{aligned} g(\mathbf{x}) &= \sum_{k \in I(\mathbf{x})} A_k \cos(\frac{z_w}{f}(u_k x \sec\rho + y v_k) + p_k) \\ &= \sum_{k \in I(\mathbf{x})} A_k \cos(\phi_k(\mathbf{x})) \approx \sum_{k \in I(\mathbf{x})} A_k \cos(\nabla\phi_k(\mathbf{x})^T \mathbf{x} + p_k). \end{aligned} \tag{6}$$

The perspective projection incurs a non-linear oscillation $\cos(\phi_k(\mathbf{x}))$ in projected image, and the local spatial frequency is approximated by taking the gradient of the phase $\phi_k(\mathbf{x})$. After substituting $\frac{z_w}{f}$ from Eq. (4), the local spatial frequency is represented in terms of the slant angle ρ :

$$\left[\frac{\partial\phi_k(\mathbf{x})}{\partial x} \;\; \frac{\partial\phi_k(\mathbf{x})}{\partial y}\right] = \left[\frac{z_0(u_k f \sec\rho - v_k y \tan\rho)}{(x\tan\rho + f)^2} \;\; \frac{z_0 v_k}{x\tan\rho + f}\right] = \left[\frac{z_0 u_k f \sec\rho}{(x\tan\rho + f)^2} + y\frac{\partial^2\phi_k(\mathbf{x})}{\partial x \partial y} \;\; \frac{\partial\phi_k(\mathbf{x})}{\partial y}\right], \tag{7}$$

where $\frac{\partial\phi_k(\mathbf{x})}{\partial x}$ and $\frac{\partial\phi_k(\mathbf{x})}{\partial y}$ correspond to frequencies in the tilt and perpendicular to the tilt, respectively. From the frequencies along the tilt and their variations perpendicular to the tilt, that is $\frac{\partial\phi_k \mathbf{x}}{\partial x}$, and $\frac{\partial^2\phi_k(\mathbf{x})}{\partial x \partial y}$, respectively, we can compute the slant angle ρ from below equation:

$$\frac{z_0 u_k f \sec\rho}{(x\tan\rho + f)^2} = \frac{\partial\phi_k(\mathbf{x})}{\partial x} - y\frac{\partial^2\phi_k(\mathbf{x})}{\partial x \partial y}. \tag{8}$$

4.3 Estimation of Surface Orientation from Ridge Surfaces

The dominant frequency variations in a projected image gives the tilt direction toward which the surface texture is slanting. We assume that surface orientation of a texture comes from a strong and smooth variations of the spatial frequency in the projected image. And, spatial frequency variations can certainly be determined from ridge surfaces. Suppose that the surface

orientation is derivable from the ridge surface $\mathcal{S}$, and $g_{\mathcal{S}}(\mathbf{x})$ is the image reconstructed by restricting the wavelet transform to $\mathcal{S}$. It is worth mentioning that $g_{\mathcal{S}}(\mathbf{x})$ may be very different from our textured image since there are surface properties in a textured image that are not captured by the ridge points in $\mathcal{S}$. To recapitulate what we have derived at Eqs. (6) and (7), $g_{\mathcal{S}}(\mathbf{x})$ is approximated by

$$g_{\mathcal{S}}(\mathbf{x}) \approx A_{\mathcal{S}} \cos(\nabla \phi_{\mathcal{S}}(\mathbf{x})^T \mathbf{x}), \tag{9}$$

where

$$\nabla \phi_{\mathcal{S}}(\mathbf{x})^T = \left[\frac{\partial \phi_{\mathcal{S}}(\mathbf{x})}{\partial x} \quad \frac{\partial \phi_{\mathcal{S}}(\mathbf{x})}{\partial y} \right] = \left[\frac{z_0 u_{\mathcal{S}} f \sec \rho}{(x \tan \rho + f)^2} + y \frac{\partial^2 \phi_{\mathcal{S}}(\mathbf{x})}{\partial x \partial y} \quad \frac{\partial \phi_{\mathcal{S}}(\mathbf{x})}{\partial y} \right]. \tag{10}$$

As mentioned in Eq. (8), slant angle ρ can be computed from the frequencies variations restricted to the ridge surface $\mathcal{S}$ in terms of $\frac{\partial \phi_{\mathcal{S}}(\mathbf{x})}{\partial x}$, and $\frac{\partial^2 \phi_{\mathcal{S}}(\mathbf{x})}{\partial x \partial y}$. The precise way of obtaining the frequency variations $\frac{\partial \phi_{\mathcal{S}}(\mathbf{x})}{\partial x}$ requires solving the partial differential equation given in Eq. (8). Since the variations of spatial frequency appears strongly along the tilt direction, it is possible to obtain a simplify way of computing $\frac{\partial \phi_{\mathcal{S}}(\mathbf{x})}{\partial x}$ by disregarding the variations of $\frac{\partial \phi_{\mathcal{S}}(\mathbf{x})}{\partial x}$ along the direction perpendicular to the tilt. It can be checked, in this case, that

$$\frac{\partial \phi_{\mathcal{S}}(\mathbf{x})}{\partial x} \quad \approx \quad (\frac{z_0}{f}) \frac{u_{\mathcal{S}} \sec \rho - v_{\mathcal{S}} \frac{y \tan \rho}{f}}{(1 + \frac{x \tan \rho}{f})^2}. \tag{11}$$

Since the spatial frequency of a textured image is characterized by ridge points, it is possible to relate $\frac{\partial \phi_{\mathcal{S}}(\mathbf{x})}{\partial x}$ to the contents of ridge points $(\mathbf{x}, s(\mathbf{x}), \theta(\mathbf{x}))$ in ridge surface $\mathcal{S}$. To recall the content of ridge point $(\mathbf{x}, s(\mathbf{x}), \theta(\mathbf{x}))$: The magnitude of the spatial frequency at $\mathbf{x}$ is inversely proportional to scale $s(\mathbf{x})$ and $\theta(\mathbf{x})$ gives the direction the frequency pointing towards. Hence, if we choose $\mathbf{k_0}$ at $(k_0 = ||\mathbf{k_0}||, 0)$; then the values of the ridge point $(\mathbf{x}, s(\mathbf{x}), \theta(\mathbf{x}))$ in the ridge surface $\mathcal{S}$ are given respectively by

$$s(\mathbf{x}) = \frac{f k_0 (1 + \frac{x \tan \rho}{f})^2}{z_0 u_{\mathcal{S}} \sec \rho} \; ; \qquad \theta(\mathbf{x}) = \tau. \tag{12}$$

It is readily clear that scale $s(\mathbf{x})$ is a parabolic function of x. Example shown in Fig. 3(b) is 3D profile of the scales in the ridge surface of a sinusoid image slanted horizontally in Fig. 3(a).

4.4 Estimation of Surface Orientation

4.4.1 Computing the tilt angle

Although the rotation θ of the ridge points $(\mathbf{b}, s, \theta)$ on the ridge surface $\mathcal{S}$ is the tilt angle τ, it is impossible to obtain this value precisely from the rotation in the ridge points. In implementation, the number of rotations used in computing the continuous wavelet transform is always limited precision by a quantization $\delta\theta$. As a consequence, we can not expect that there will be enough number of rotations available for determining the tilt angle to any precision. However, we know earlier that ridge surface $\mathcal{S}$ parameterized in scale is a parabola(see Eq. 12), depending on the value of the tilt τ, slant ρ, and coordinates x_i and y_i. The parabola is a canonical form provided that we represent it using the new coordinate system $\mathbf{x}$, obtained by rotating $\mathbf{x_i}$ exactly τ degrees. We denote the ridge points $([x_i, y_i]^T, s_i, .)$ on $\mathcal{S}$. To estimate the tile angle, we fit the ridge surface $\mathcal{S}$ by using the quadratic function of x_i and y_i,

$$P(x_i, y_i) = a_1 x_i^2 + a_2 x_i y_i + a_3 y_i^2 + a_4 x_i + a_5 y_i + a_6.$$

We know that the above formula can be expressed in the canonical form:

$$P^{'}(x, y) = \tilde{a_1} x^2 + \tilde{a_4} x + \tilde{a_6},$$

where the mixed-product term is eliminated by a rotation of τ degrees of the coordinate system. The new formula $P^{'}(x, y)$ is independent of the axis y, which is pointing in the direction perpendicular to that of the tilt. It is a simple matter to obtain the tilt angle of $\mathcal{S}$ from the following formula:

$$\tau = \tan^{-1} \frac{a_5}{a_4}. \tag{13}$$

4.4.2 Computing the slant angle

Computation of slant angle by voting method From Eq. 12, the slant angle ρ can be solved from the quotient of the scales $s([x_1, y_0]^T)$ and $s([x_2, y_0]^T)$ of two points in a ridge curve (with constant y) given by

$$\frac{s([x_1, y_0]^T)}{s([x_2, y_0]^T)} = \frac{(1 + \frac{x_1}{f} \tan\rho)^2}{(1 + \frac{x_2}{f} \tan\rho)^2} = C^2.$$

Solving the above equation for ρ, we have the slant angle:

$$\rho = \tan^{-1}(\frac{f(1-C)}{Cx_2 - x_1}), \tag{14}$$

where $C = \sqrt{\frac{s([x_1,y_0]^T)}{s([x_2,y_0]^T)}}$.

Computation of slant angle by curve fitting The ridge curve is approximated by $\beta_2 x^2 + \beta_1 x^1 + \beta_0$. Equating the coefficients of the above two equations, the slant angle is related to the three coefficients β_0, β_1, and β_2. After simple calculation, the slant angle ρ is derived by

$$\rho = \tan^{-1}(\frac{f\ \beta_1}{2\beta_0}). \tag{15}$$

5 Robust Estimation

Fig. 4(a) shows an image of sinusoid containing only one frequency. Fig. 5(a) shows the modulus of the wavelet transform at various orientations with respective to the scale at a given location. It is found that the energy is appeared in one orientation and concentrated on a narrow band of frequency. The peak frequency of this location is fairly apparent. It is enough to represent the frequency of this location by the peak frequency. Unfortunately, there is few image like sinusoid image encountered in the real-world. According to Rao's book [17], the textured images can be roughly categorized into three classes: strongly ordered, weakly ordered, and disordered textures. All these textures can be regarded as the images composed of multiple frequencies. Fig. 4(b) shows an strongly ordered texture D95. Similarly, the modulus responses with respect to scale at one location are shown in Fig. 5(b). We see that the energy appears more than one orientations and concentrated on some frequency bands. But, it is still easily to choose local peak frequencies as the "signature" of the local texture variations. Moreover, the neighboring pixels in regular textures usually have similar frequency responses and, thus, the multiple ridge algorithm gives us nice continuous ridge surfaces which tend to separate different frequency components, see Fig. 1. However, for the weakly ordered and disordered textures shown in Figs. 4(c) and (d), the spatial frequency distributions become much more complex and the neighboring pixels tends to have different frequency distributions in each orientation(see

Figs. 5(c) and (d)). In such cases, the multi-ridge detection algorithm is unable to determine "good" continuous ridge surfaces. Therefore, some constraints are necessary to be imposed on the ridge points in determining the surface orientation. The constraints we found are the consistency of orientation and the outlier detection for scales.

Consistency of orientation: When a perceived image is slanted, the representative orientations of ridge points should be consistent with the tilt angle as possible. All the ridge points violate the consistency are discarded from the ridge surface.

Outlier detection in scales: As described in the previous section 3, the ridge points are fitting into a parabola. To have a robust fitting, the outlier points shoud be eliminated. A robust regression method such as RANSAC [10] is applyed in our parabola fitting. This outlier detection is particularly useful for the weakly and disordered textures as Fig. 7 shows.

6 Experiments

The textured images used in our experiments mainly come from Brodatz's album [7] and images obtained from WWW. The Morlet wavelet with center frequency $k_0 = 6.9$ was used. Four octaves, eight voices, and eight rotations to perform the continuous wavelet transform. The experimental results using Algorithm 2 (Mulit-ridge detection) have average error of tilt angle within 1.48°, and the average errors of slant angle using the voting and curve fitting within 2.18° and 2.75°, respectively. Furthermore, the capability of noise-tolerance of Algorithm 2 have been demonstrated for some noisy images with various SNR ranging from 20 db to -5 db. We find that the estimated results were almost the same as those of the noise-free images. In order to save the space, the textured images and their detected ridges are not shown here. They can be found in [12]. On the other hand, we perform a similar as Turner [19] by our robust estimation method. The three same images D95, D84, D24 are slanted 15°, 30°, 45°, 60°, and 75°, respectively. The estimated slant angles are shown in Fig. 6. It is found that estimated slant angles are close to the true slant angles except for the D84 image (slanting 75°). In addition, the textured images used for robust estimations (Sec. 5) are shown in Fig. 7(a)-(h). It is seen that the structures of these images are not apparent. Among them, D04,

D09, and D92 belong to disordered textures, while D15 and D24 are weakly ordered textures according to the Rao's book [17]. Their estimated results are shown in Table 1. The average error of tilt is within 4.46° and those of slant angles using voting and curve fitting are within 2.56° and 3.89°, respectively. Fig. 8 shows the examples of the single ridges and the inliers (after robust regression) of Fig. 7(a) and Fig. 7(f). Comparing the single ridge and the inlier, it is found that the useful information are kept.

7 Conclusions

We have proposed two new methods for estimating the orientation of a planar surface texture under the perspective projection model. Texture variations are effectively characterized by local frequencies based on continuous wavelet transform. Even though a textured image has more than a single dominant frequency component, the proposed multiple ridge detection algorithm is able to choose the ridge surface that describe the surface orientation. For some natural textures, mostly weakly ordered and disordered, the surface orientation can not be determined accurately from ridge surfaces. We proposed a random regression method together with the single ridge detection algorithm to solve the problem. The effectiveness of our method has been demonstrated on several real-world images.

References

[1] J. Aloimonos, "Shape from texture", *Biological Cybernetics*, Vol. 58, 1988, pp. 345-360.

[2] J. -P. Antoine, P. Carrette, R. Murenzi, and B. Piette, "Image analysis with two-dimensional continuous wavelet transform", *Signal Processing*, Vol. 31, 1993, pp. 241-272.

[3] R. Bajcsy and L. Lieberman, "Texture gradients as a depth cue", *Computer Graphics and Image Processing*, 1976, pp. 52-67.

[4] A. Blake and L. Lieberman, "Shape from texture: Estimation, isotropy, and moments", *Artificial Intelligence*, Vol. 45, 1990, pp. 323-380.

[5] D. Blostein and N. Ahuja, "Shape from texture: Integrating surface element extraction and surface estimation", *IEEE Trans . Pattern Anal. and Machine Intell.*, Vol. 11, 1989, pp. 1233-1251.

[6] A. C. Bovik, N. Gopal, T. Emmoth, A. Restrepo(Palacios), "Localized measurements of emergent frequencies by Gabor wavelets", *IEEE Trans. Inform. Theory*, Vol. 38, 1992, pp. 691-712.

[7] P. Brodatz, "Textures: A photographic album for artists and designers", *Dover Publications*, 1966.

[8] L. G. Brown and H. Shvaytser, "Surface orientation from projective foreshortening of isotropic texture autocorrelation", *IEEE Trans . Pattern Anal. and Machine Intell.*, Vol. 12, 1990, pp. 584-588.

[9] N. Delprat, B. Escudie, P. Guillemain, R. Kronland-Martinet, P. Tchamitchian, and B. Torrésani, "Asymptotic wavelet and Gabor analysis: Extraction of instantaneous frequencies", *IEEE Trans. Inform. Theory*, Vol. 38, No. 2, 1992, pp. 644-664.

[10] M. A. Fischler and R. C. Bolles, "Random Sample Consensus: A Paradiam for Model Fitting with Applications to Images Analysis and Automated Cartography", *Communications of ACM*, Vol. 24, 1981, pp. 381-395.

[11] J. Gibson, "The Perception of the Visual World", Houghton Mifflin: Boston, 1950.

[12] W. L. Hwang, C. S. Lu and P. C. Chung, "Shape From Texture: Direct Estimation of Planar Surface Orientation Using Continuous Wavelet Transform", *Submitted to IEEE Transaction on Image processing*, also TR-IIS-96-015 of Institute of Information Science, Academia Sinica, Taiwan, R.O.C.

[13] Y. C. Jau and R. T. Chin, "Shape from texture using the Wigner distribution", *Comput. Vision Graphics Image Proces.*, Vol. 52, 1990, pp. 248-263.

[14] J. Krumm and S. Shafer, "Shape from periodic texture using the spectrogram", *Proc. Conf. Computer Vision and Pattern Recognition* , 1992, pp. 284-289.

[15] P. Kube, "Using Frequency and Orientation Tuned Channels to Determine Surface Slant", *Eight Annual Conference of the Cognitive Society, Amherst, Massachusetts*, 1986, pp. 235-244.

[16] C. S. Lu, W. L. Hwang, H. Y. Mark Liao, and P. C. Chung, "Shape from texture based on the ridge of continuous wavelet transform", *IEEE Inter. Conf. on Image processing*, Vol. I, 1996, pp. 295-298.

[17] A. Ravishankar Rao, "A Taxonomy for Texture Description and Indetification", *Springer Verlag*, 1990.

[18] B. Super and A. C. Bovik, "Planar surface orientation from texture spatial frequencies", *Pattern Recognition*, Vol. 28, No. 5, 1995, pp. 729-743.

[19] M. R. Turner, G. L. Gerstein, and R. Bajcsy, "Underestimation of visual texture slant by human observers: a model", *Biological Cybernetics*, Vol. 65, 1991, pp. 215-226.

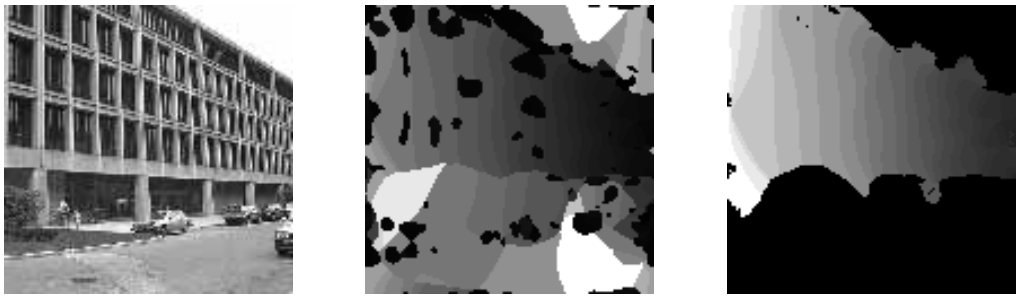

(a) A scene (b) Single ridge (c) Multiple ridge 1

(d) Multiple ridge 2 (e) Multiple ridge 3 (f) Multiple ridge 4

Figure 1: Multi-ridge detection of a scene.

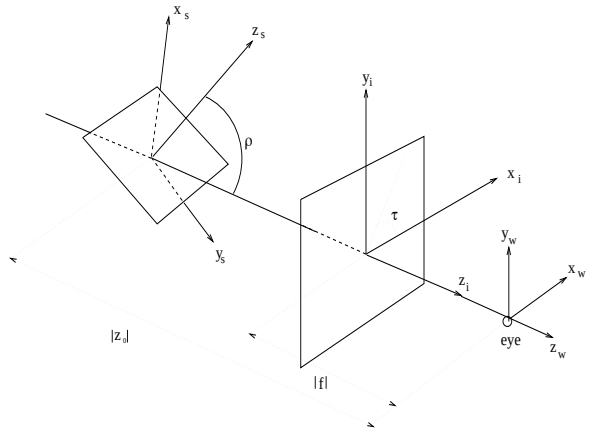

Figure 2: The coordinate relationship between the image plane and the surface plane with slant angle ρ and tilt angle τ.

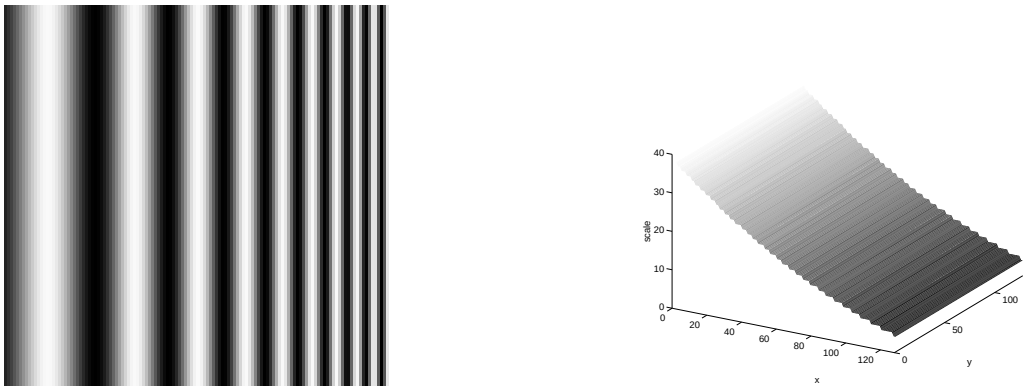

(a) (b)

Figure 3: Slanted cosine image and 3-D plot of its ridge: (a) The slanted image; (b) 3-D scale map of the ridge.

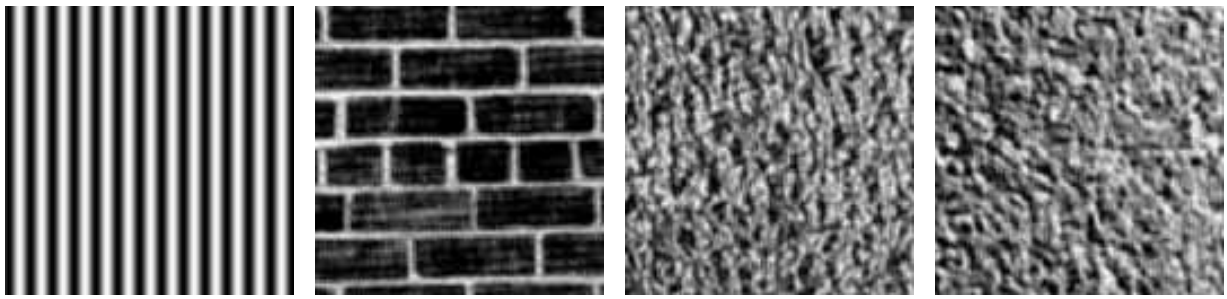

(a). Sinusoid image (b). D95 (c). D24 (d). D04

Figure 4: Various structured images: (a) Sinusoid image; (b) Strongly ordered texture; (c) Weakly ordered texture; (d) Disordered texture.

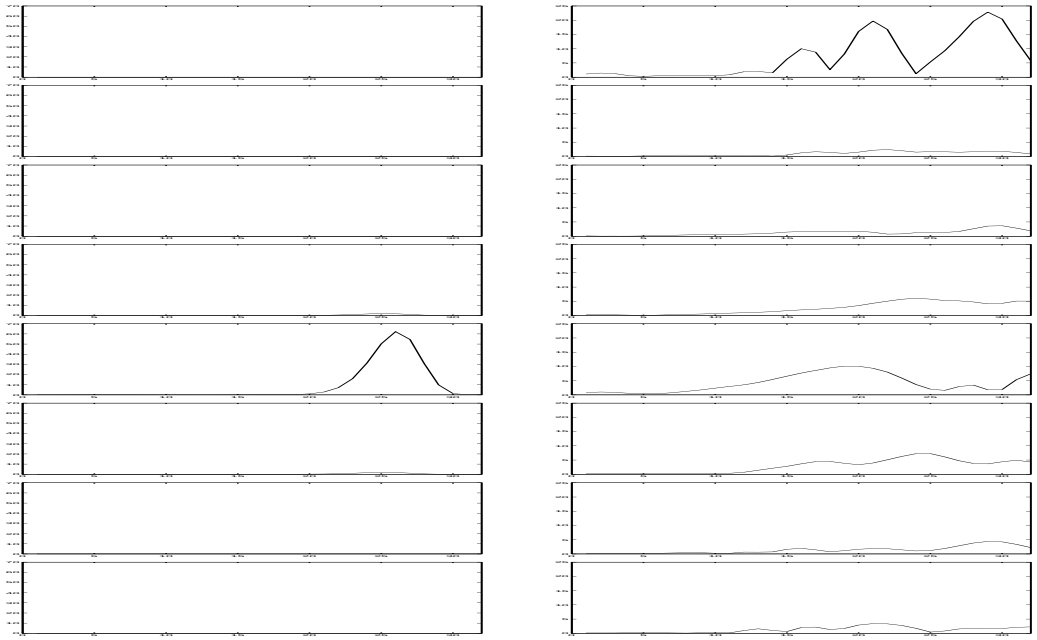

4(a)

4(b)

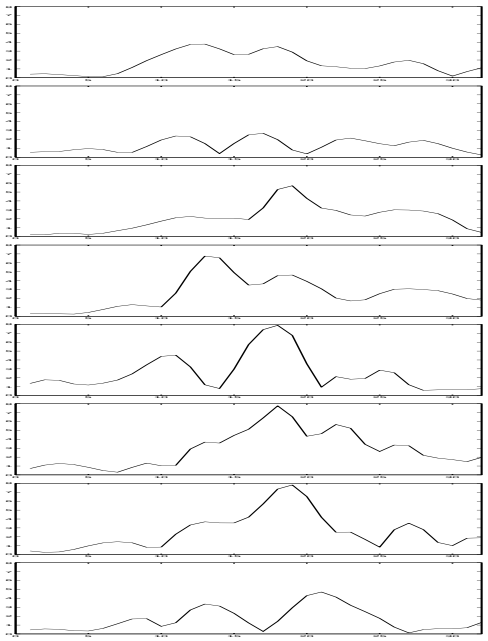

4(c)

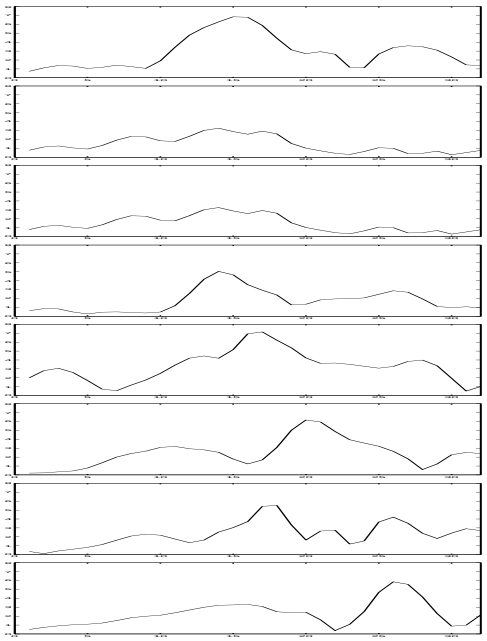

4(d)

Figure 5: The modulus of wavelet transform with respect to scale at various orientations of a location: (a) Sinusoid image, (b) D95, (c) D24, and (d) D04. The scale increases from the left to the right horizontally, modulus is indicated vertically; and the subplot boxs show the orientations from $-90°$, $-67.5°$, ..., $67.5°$(top to bottom)

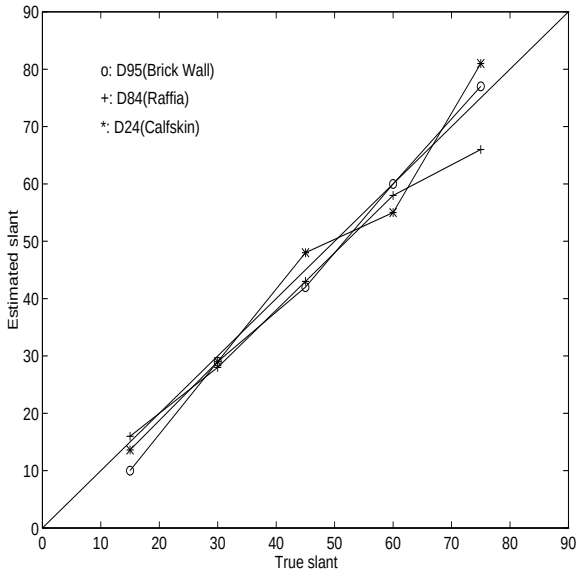

Figure 6: Estimations for three natural textures D95, D84, and D24 slanted 15°, 30°, 45°, 60°, and 75°.

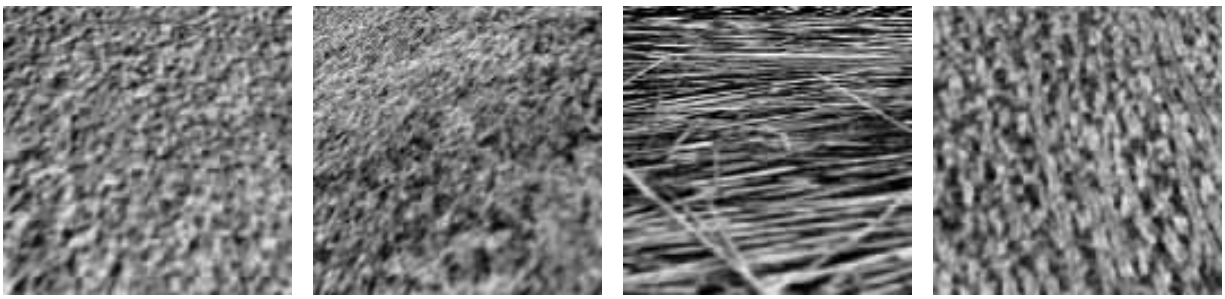

(a). D04 (b). D09 (c). D15 (d). D24

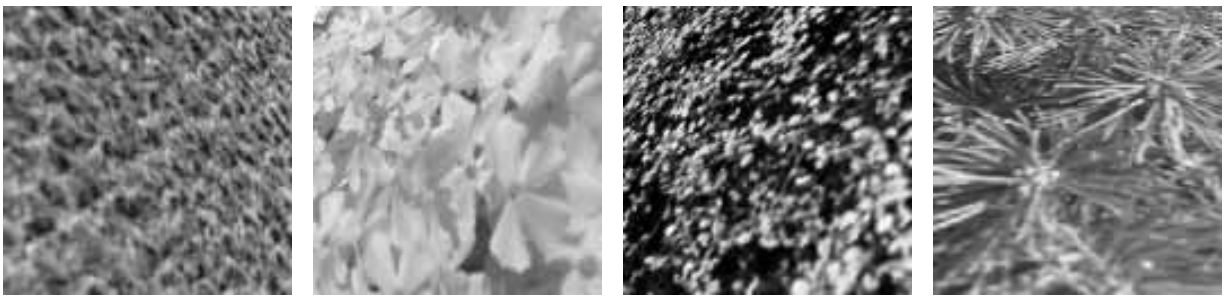

(e). D92 (f). Flowers (g). Leaves-1 (h). Leaves-2

Figure 7: Test images.

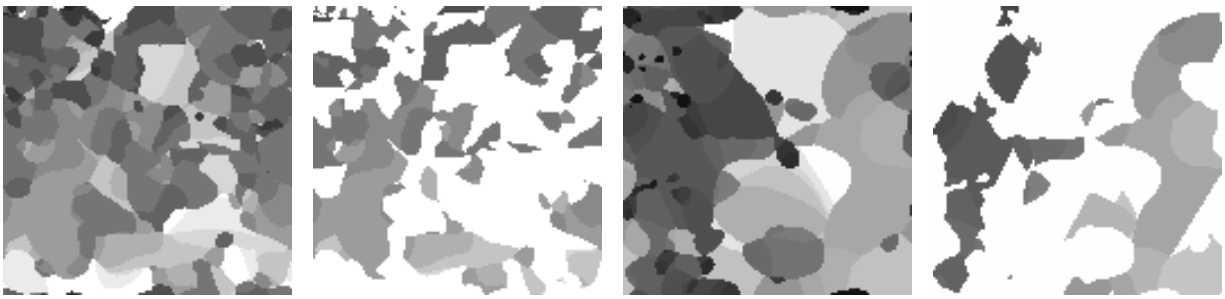

(a).D04:single ridge (b).D04:inlier of (a) (c).Flowers:single ridge (d).Flowers: inlier of (c)

Figure 8: Examples of single ridges and their inliers for D04 and Flowers

Table 1: **Estimated surface orientation.**

Image	$True\tau$	τ_m	$\mid \tau_m - \tau \mid$	$True\rho$	ρ_v	ρ_c	$\mid \rho_v - \rho \mid$	$\mid \rho_c - \rho \mid$
D04	90	95.47	5.47	30	29.00	30.33	1.00	0.33
D09	120	109.88	10.12	50	50.00	45.08	0.00	4.92
D15	0	-2.25	2.25	55	50.00	50.20	5.00	4.80
D24	60	56.11	3.89	15	14.00	12.82	1.00	2.18
D92	45	36.03	8.97	40	44.00	43.39	4.00	3.39
Flowers	150	150.63	0.63	45	43.00	39.00	2.00	6.00
Leaves-1	135	134.02	0.98	45	38.00	37.24	7.00	7.76
Leaves-2	90	85.94	4.06	50	49.50	48.26	0.50	1.74

τ_m: tilt angle of our method

ρ_v: slant angle of our voting method

ρ_c: slant angle of our curve fitting method